remote sensing

MDPI

Article

An Investigation into Land Surface Temperature-Based Climate Indices

Josh Blannin [1,*,†], Elizabeth Good [1], Carlos Jimenez [2,3] and Arno Cheda [4,5]

[1] Met Office Hadley Centre, Exeter EX1 3PB, UK; elizabeth.good@metoffice.gov.uk
[2] Estellus, 75002 Paris, France; carlos.jimenez@estellusmw.fr
[3] LIRA, Observatoire de Paris, PSL Research University, CNRS, Sorbonne Universités, Univ. Paris Cité, 75014 Paris, France
[4] Federal Office of Meteorology and Climatology, MeteoSwiss, 8058 Zurich, Switzerland; arno.cheda@meteoswiss.ch
[5] Department of Environmental Systems Science, ETH Zurich, 8093 Zurich, Switzerland
* Correspondence: jmb289@exeter.ac.uk
† Current address: Department of Geography, Faculty of Environment, Science and Economy, University of Exeter, Exeter EX4 4QE, UK.

Highlights

What are the main findings?

- Climate indices based on near-surface air temperature and satellite land surface temperature are compared globally.
- Climate indices from near-surface air temperature and land surface temperature show strong similarities

What are the implications of the main findings?

- Climate events, such as heatwaves, may be identified from land surface temperature indices
- Climate indices from land surface temperature can be informative and should be used in conjunction with indices produced from near-surface temperature.

Abstract

Monitoring climate change is crucial to society, industry, and the environment to assess their vulnerability to such extreme temperature events and plan adaptation and mitigation strategies. Temperature-based climate indices, which are used for climate monitoring, are usually calculated using near-surface air temperature (NSAT) from weather stations. A limitation of NSAT is the inhomogeneity of station distribution across the globe, with some regions under-sampled. This study evaluates the potential of using land surface temperature (LST) retrieved via satellite to calculate temperature indices, because low Earth-orbiting satellites can observe almost all of the Earth. This work compares indices calculated from NSAT to those produced from LST, and the indices are aggregated by Intergovernmental Panel on Climate Change AR6 regions. Results show that there is often moderate to high correlation between indices produced using NSAT and LST. In addition, it is found that monthly to seasonal changes in indices are similar for both variables, particularly in percentile-based indices. Threshold-based indices could not be calculated for some regions due to low data availability, and therefore this work also applies "relative" indices, where indices are normalised relative to the amount of data available. These generally also demonstrate high correlations between NSAT and LST and can better show when events, such as heatwaves, occur. Lastly, this work presents the potential of an LST-based temperature indices dataset and how uncertainties could be evaluated.

Check for updates

Academic Editor: Donglian Sun

Received: 30 June 2026
Revised: 30 September 2026
Accepted: 15 October 2026
Published: 6 November 2026

Copyright: © 2026 by the authors. Licensee MDPI, Basel, Switzerland. This article is an open access article distributed under the terms and conditions of the Creative Commons Attribution (CC BY) license.

Keywords: climate indices; land surface temperature; climate change initiative; European Space Agency; heatwaves; climate monitoring

1. Introduction

The Intergovernmental Panel on Climate Change (IPCC) 6th Assessment Report (AR6) states that climate change will impact the occurrence of extreme weather events, and that "CMIP6 simulations show that a 0.5 °C increment in global warming will significantly increase the intensity and frequency of hot extremes" [1]. This has already been seen in the record number of globally averaged warm days and maximum temperatures (see "Surface Temperature Extremes" in [2]), and an increasing trend in these metrics across Earth [3]. This is of significant concern as temperature extremes can have substantial negative impacts on human and animal mortality [4–6], agriculture [7,8], and critical infrastructure [9]. Given the current warming trend, observations of temperature-related climate variables are vital in monitoring the frequency, intensity and duration of extremes, and aid in identifying regions which are vulnerable to such events, as well as evaluating model projections. The WMO (World Meteorological Organisation) ETCCDI (Expert Team on Climate Change Detection and Indices) compiled and developed a suite of 27 climate indices for the purpose of climate monitoring. Several of these indices are related to moderate extremes which can be infrequent (but not rare) and may not have significant consequences. The indices are internationally agreed, simple and feasible to calculate, and allow the sharing of climate information without having to release daily or sub-daily data [10,11]. This selection of indices was expanded upon by the WMO Expert Team on Sector-Specific Climate Indices (ET-SCI).

A number of datasets have been established to provide gridded climate extremes indices for the globe, such as GHCNDEX [12] and HadEX (currently on its third version, HadEX3) [3,13], with temperature-related indices produced from station-based near-surface (typically 1.5–2 m above ground) air temperature (NSAT) observations. These indices are gridded onto 2.5° × 2.5° and 1.875° × 1.25° longitude-latitude grids for GHCNDEX and HadEX3, respectively. However, a key limitation of any station-based dataset is the inhomogeneous distribution of stations across the globe. For example, there are far fewer stations in the African continent than in Europe or North America. Additionally, when quality control measures are applied to station records, many are discarded due to unreliable data, non-climatic discontinuities (inhomogeneities), or having too short a timeseries, further increasing station sparsity. Once gridded, this leads to greater uncertainties in grid cell values for those with fewer observations, or spatio-temporal gaps in a "global" land dataset.

This study uses satellite LST data for computing climate temperature indices. Near-surface air temperature (referred to as "air temperature" from here on) cannot be measured from space; however, satellites can be used to retrieve the land surface temperature (LST), which is the mean radiative skin temperature of the objects within the sensor field of view [14]. The use of remotely sensed LST is motivated by the fact that satellite retrievals can overcome some of the limitations posed by gridded station-based air temperature index products. LST is derived from the surface emission integrated over an area corresponding to the ground footprint of the satellite instrument. Here, data retrieved from microwave sensors onboard low Earth-orbiting (LEO) satellites are used. These satellites travel in orbits that pass close to the poles and observe nearly all points of the Earth, overcoming a major limitation posed by gridded station-based air temperature index products. The satellite revisit times, i.e., the time it takes for the satellite to view a point it has previously

observed, can be sub-daily at the poles due to overlapping swaths, but closer to 2–3 days along the equator. Whilst this frequency will always be longer than the reporting interval of stations, even revisit periods of a couple of days would provide more data in regions that have too few stations to robustly produce indices for a given grid cell. Satellite LST products can also have a greater spatial resolution than gridded air temperature index products and be easier to quality control than thousands of individual station observations. However, a limitation is that any systematic biases or discontinuities from sensor changes or calibration drifts are harder to address and may require complex homogenisation procedures.

This study computes climate indices using LST and assesses how similar these are to indices derived from air temperature. In Section 2, the methodology is presented, describing the air temperature and LST datasets used, as well as the climate indices assessed. Section 3 presents the results of the indices computed using LST and air temperature. The results are summarised across the regions defined by the IPCC AR6. Section 4 assesses the performance of the LST indices and evaluates the similarities and differences with air temperature indices. In addition, Section 4 also discusses how well the LST indices are represented in regions with lower data availability, and whether they capture climate extremes by looking at a selection of historical events. There is also discussion on producing an LST-based index dataset and deriving the relevant uncertainties. Section 5 concludes the study and reviews the findings. Lastly, the Supplementary Materials holds figures referred to in Sections 3 and 4 but not shown within the main text.

2. Materials and Methods

This section presents the data processing methodology and the definitions and requirements of the climate indices used in this study. A graphical representation of the methods can be found in the Supplementary Materials (Figure S1).

2.1. Station Data

The station dataset used in this study is the Global Historical Climatology Network daily (GHCNd) [15]. GHCNd, compiled by the National Oceanic and Atmospheric Administration (NOAA), is a multivariate dataset of meteorological variables from more than 100,000 stations in 180 countries and territories. Metadata and daily air temperature maximum (T_{max}) and minimum (T_{min}) are acquired for each station from its respective Global Summary of the Day. The stations are grouped into areas defined for the Intergovernmental Panel on Climate Change (IPCC) 6th Assessment Report (AR6) regions [16,17] using shape files provided in [18]. Checks are carried out on the station data to ensure measurement dates are available along with at least one of T_{max} or T_{min} and that the respective quality flag was empty (indicating the data was not suspect). Data are removed if the quality flags indicate an unreliable value, or if the quality flags are in the wrong format. Only data recorded between 1996 and 2020 are used to align with the available satellite period, and a minimum of 365 days of data (T_{max} and T_{min} combined) is required to ensure the station was operational for at least a year within that period. If $T_{max} \leq T_{min}$, both values are dropped, and leap days are also removed to keep the number of days consistent across all years. Figure 1 shows the location of the 23,249 stations with data suitable for this study.

2.2. Land Surface Temperature Data

Radiometers operating at thermal infrared (TIR) and microwave (MW) wavelengths onboard satellites measure the radiances required for deriving LST. Using TIR to estimate LST gives a higher spatial resolution compared to MW; for example, TIR from the Moderate Resolution Imaging Spectroradiometer (MODIS) is at a resolution of 1 km [19], whereas typical MW imagers are closer to 10–20 km [20]. However, a major disadvantage of using

TIR is that these wavelengths cannot penetrate clouds, whereas microwaves are far less affected [21]. With global annual mean cloud area fraction greater than 68% during the satellite era (see "Cloudiness" in [2]), there is more LST data available from microwave sensors. Given that larger sample sizes lead to more robustly computed climate indices, MW-based LST is used in this study over TIR due to its greater data availability.

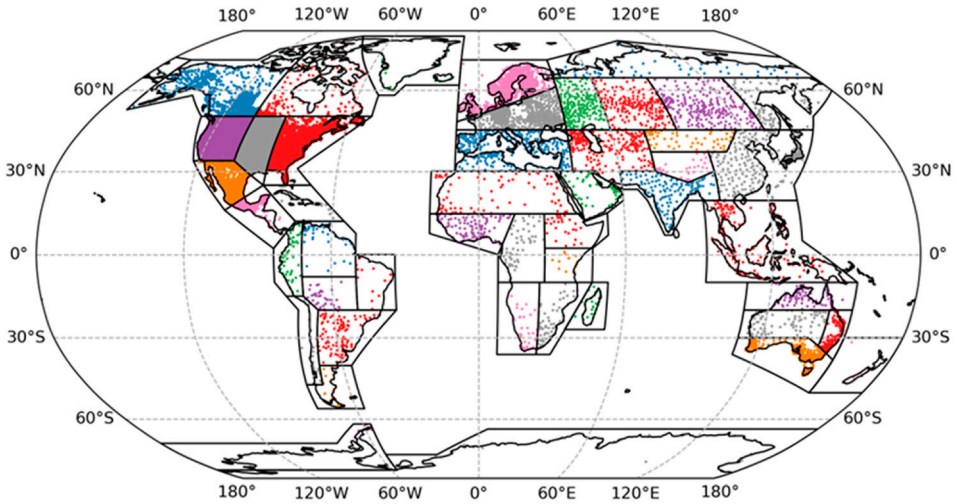


Figure 1. GHCNd stations within AR6 land regions available to this study following quality control. Total number available is 23,249. Colours distinguish between AR6 regions (colours are not unique to a region; repeat colours are used). Filled regions are due to overlapping points due to high station density.

Satellite LST data are from the European Space Agency (ESA) Climate Change Initiative for Land Surface Temperature (LST_cci). This work uses version 2.33 of the ESA LST_cci All-weather Microwave (MW) Land Surface Temperature global data record [22]. Although later versions of this dataset are available, they are not used here due to issues with stability in these versions as a result of using different sources for the input MW radiances.

LST from MWs is considered near all-sky because, although atmospheric attenuation of low-frequency microwaves (≤37 GHz), including by clouds, is relatively small when compared to the emission from the land surface, clouds can impact the high-frequency channels (≥89 GHz) and those containing large ice particles (i.e., deep convective clouds), which scatter the microwaves, causing a reduction in LST accuracy [23]. The radiances used to derive MW LST are measured by the Special Sensor Microwave/Imager (SSM/I) and the Special Sensor Microwave Imager/Sounder (SSMIS) onboard the Defence Meteorological Satellite Programme F13 and F17 satellites, respectively. These satellites are subject to orbital drift resulting in a change in local observing time over the satellite record. To mitigate this issue, a correction value, packaged with the data, is applied to adjust the data to 6 AM/PM local time. For the remainder of this manuscript, the corrected data will be referred to as either the "nighttime overpass" or "daytime overpass", referring to the data adjusted to 6 AM/PM respectively. Quality flags are supplied in a bitwise manner, and any that comprise the 32 and 64 flags are excluded, which has the effect of removing data from Microwaves produced within deep convective storms and those from coastal regions (which are contaminated by signals from water) [24]. Stations are co-located with the single LST grid cell that contains the station coordinates, producing daytime and nighttime LST timeseries. Typically, the LST measured during the daytime overpass is greater than that from the nighttime overpass; however, this is not always the case in the event of passage of a cold (warm) front during the day (night). Therefore, to make consistent comparisons with air temperature, whichever of the daily daytime LST (LST_{day}) and nighttime LST (LST_{night})

is greater is compared with T_{max} and the lesser with T_{min}. When only one of LST_{day} or LST_{night} is available, LST_{day} is compared with T_{max} and LST_{night} is compared with T_{min}, following the approach in [25].

2.3. Climate Indices

The climate indices used in this study (Table 1) are a subset of the indices recommended by ET-SCI with the addition of four new percentile-based indices (TX5p, TX95p, TN5p and TN95p). Table 1 shows the indices used and their respective definitions, where TX and TN represent whether the index is computed using the daily maximum or minimum temperatures, respectively. This study classifies the indices into three types: value-based, threshold-based, and percentile-based. Value-based indices produce a statistical measure of the temperature, threshold-based indices show the number of days when the temperature exceeds a predetermined value, and percentile-based indices are the proportion of days when the temperature exceeds a calculated percentile. The index frequencies are provided in the ETCCDI and ET-SCI definitions for value-based indices and threshold-based indices, which are monthly and annual, respectively. The percentile-based indices used in this study are chosen to be monthly, as the definitions do not formally set a frequency and monthly indices provide more information on temporal variability.

Table 1. Notation, type, and description of computed indices. TX and TN represent whether the index is computed using the daily maximum or minimum temperatures, respectively.

Index	Index Type	Description
TXx	Value	Monthly maximum value of TX
TXn	Value	Monthly minimum value of TX
TXm	Value	Monthly mean value of TX
TNx	Value	Monthly maximum value of TN
TNn	Value	Monthly minimum value of TN
TNm	Value	Monthly mean value of TN
SU	Threshold	Annual count of days when TX > 25 °C
ID	Threshold	Annual count of days when TX < 0 °C
TN	Threshold	Annual count of days when TN > 20 °C
FD	Threshold	Annual count of days when TN < 0 °C
TNlt2	Threshold	Annual count of days when TN < 2 °C
TNltm2	Threshold	Annual count of days when TN < −2 °C
TNltm20	Threshold	Annual count of days when TN < −20 °C
TXge30	Threshold	Annual count of days when TX ≥ 30 °C
TXge35	Threshold	Annual count of days when TX ≥ 35 °C
TX5p	Percentile	Monthly percentage of days when TX < 5th percentile
TX10p	Percentile	Monthly percentage of days when TX < 10th percentile
TXgt50p	Percentile	Monthly percentage of days when TX > 50th percentile
TX90p	Percentile	Monthly percentage of days when TX > 90th percentile
TX95p	Percentile	Monthly percentage of days when TX > 95th percentile
TN5p	Percentile	Monthly percentage of days when TN < 5th percentile
TN10p	Percentile	Monthly percentage of days when TN < 10th percentile
TNlt50p	Percentile	Monthly percentage of days when TN < 50th percentile
TN90p	Percentile	Monthly percentage of days when TN > 90th percentile
TN95p	Percentile	Monthly percentage of days when TN > 95th percentile

Percentiles for the percentile-based indices are calculated for each calendar day using all data within a 5-day window over the study period and are produced separately for the air temperature and LST data. As the 1996–2020 study period does not exceed the typical reference period timescale of 30 years, the bootstrapping method in [26], used to remove inhomogeneities between in- and out-of-reference period indices, is not applied in

the custom software (v1.0) [27] developed for this study; i.e., the entire 25-year record is considered as the reference period. TX5p, TX95p, TN5p and TX95p are not ET-SCI indices but follow the same methodology as the other percentile-based indices, instead using the 5th and 95th percentiles as thresholds. These are added to explore temperature extremes that may cause greater impacts across society and industry.

Whilst custom software was used, to ensure robustness of the indices, the data availability requirements for this study are guided by those used in the Climpact software, which was developed to calculate air temperature indices [28]. The requirements set in the current version of Climpact (v3.3) are:

1. Maximum of 3 missing days in monthly indices—approx. 90% data availability;
2. Maximum of 15 missing days in annual indices—approx. 96% data availability;
3. Do not compute annual indices if any month has more than 3 missing days;
4. 10% of the base-period must contain valid values for percentile-based indices to be calculated.

For annual indices, requirements 2 and 3 are rarely met for LST data, except at very high latitudes (Figure 2), largely due to swath gaps in the satellite LST data but also because of data removed from grid cells flagged with suspect data (Section 2.2). Therefore, requirement 2 is relaxed to "Maximum of 36 missing days in annual indices" and requirement 3 is dropped to allow for indices in more regions to be derived. In addition, this study raises the percentage of data needed for percentile-based indices to be calculated (requirement 4) to 70%, to ensure robust percentiles are calculated.

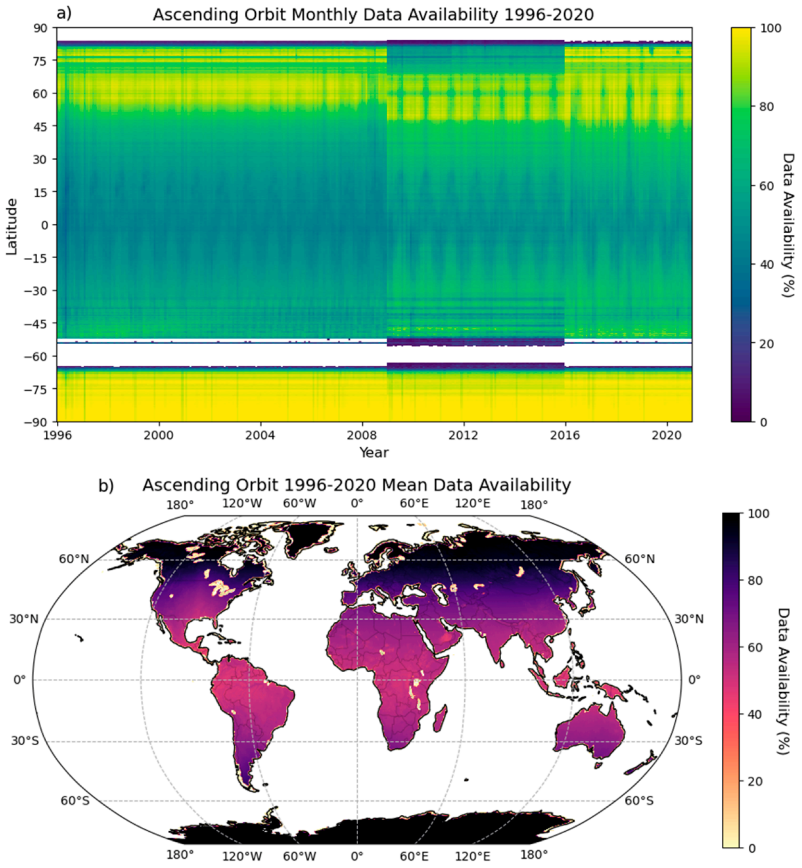


Figure 2. *Cont*.

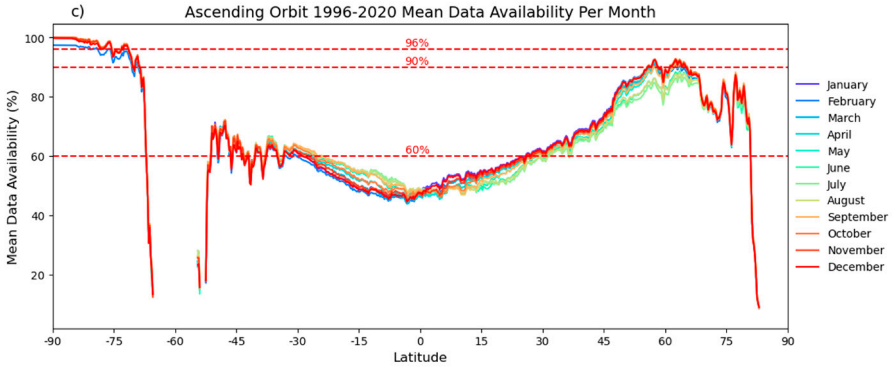


Figure 2. Data availability for the LST_cci Microwave product with flagged data removed (Section 2.2): (**a**) Hovmöller plot showing monthly data availability averaged (mean) over longitudes between 1996 and 2020; (**b**) global map of the total data availability between 2019 and 2026; and (**c**) data availability per month averaged (mean) between 1996 and 2020 and over longitudes. The variability in (**a**) is due to satellite orbit swath gaps and removal of grid cells indicated as coastal or inundated with water (Section 2.2). Additionally, in (**a**) the discontinuity in 2009 is a result of the transition from SSM/I to SSMIS, and the cause of the step change at the end of 2015 is currently unknown. Dashed red lines in (**c**) indicate data availability requirements to calculate indices (Section 2.3).

A limitation with LST retrieved from polar-orbiting satellites is that gaps between swaths increase towards the equator, resulting in less frequent observations. There are also coastal areas where data can often be removed due to water contaminating the grid cells. To account for the reduced data coverage, relative indices are explored. This is a concept used in Cheda et al. (2026) [29] and represents the proportion of temperature measurements that exceed the threshold out of the amount of data available. The rationale for this is to remove the bias in the LST threshold-based indices that occurs due to a lower sampling frequency closer to the Equator. For example, consider a 10-day period where both Tmax and LSTday exceed 25 °C for all days. The standard Summer Days index for air temperature (SUair-std) would be SUair-std = 10. But if the LST data availability were only 50%, the LST Summer Days index (SULST-std) would be SULST-std = 5, introducing a 5-day bias. However, by considering the number of days relative to the amount of data available, the relative Summer Days indices for air temperature and LST (SUair-rel and SULST-rel, respectively) yield: SUair-rel = 10/10 = 1.0 and SULST-rel = 5/5 = 1.0, which better represents the true situation within the data availability limitations. To be able to calculate relative indices for more regions, the data availability threshold is reduced to 60%, allowing these to be produced for some regions south of ~15°S and north of ~30°N with data from the current SSMIS microwave sensor (Figure 2c). A single (60%) threshold is used in this study to demonstrate and test the use of relative indices, but note that future development of an LST indices dataset could include a sensitivity test of applied thresholds. Additionally, whilst the use of relative indices resolves the problems due to missing data resulting from swath gaps, this does not mean biases have been completely removed. For example, deep convective storms can result in microwave LST data being excluded, and therefore climate extremes may be missed where these weather patterns are having a direct influence. As such, a systematic bias may still be present in some circumstances.

To assess the similarity between air temperature and LST indices, results from each AR6 region (Figure 1) are grouped and averaged through a simple arithmetic mean. However, it should be noted that the regional index means do not necessarily reflect the "true" mean for the entire AR6 region, due to the heterogenous spatial distribution of stations. For this study, the focus is not on the "true" regional index means but rather on investigating whether the indices derived from two independent datasets are similar and broadly show the same climate signals. Pearson correlations between the air temperature and LST indices

are calculated using the *pearsonr* function from the SciPy package v.1.15.2, which provides confidence intervals using the Fisher transformation. A minimum of 30 co-located index values is required to compute the Pearson correlation coefficient. For value-based indices, correlation coefficients are calculated from the monthly anomalies to remove any seasonal effects. These monthly anomalies are calculated by subtracting a climatology for each index, calculated from the mean for each calendar month observed during the baseline period 1996–2020. The same baseline period is used for both the NSAT and LST value-based indices. Correlation coefficients for threshold- and percentile-based indices are computed from the actual index values, as the threshold-based indices are annual (in this case), meaning there are no seasonal effects, and percentile-based indices are self-normalised.

3. Results

This section reports the results produced for the value-, threshold-, and percentile-based indices. This study utilises 25 climate indices and applies them to 46 AR6 regions, leading to a total of 1150 separate results. Regional correlations (r) are calculated where at least 30 valid spatially and temporally co-located index values are available for both air temperature and LST. The following sections provide a summary of the findings and highlight important features.

3.1. Value-Based Indices

The value-based indices typically show a good correlation across all indices for the AR6 regions with sufficient data to compute this statistic. A subset of available regions across different continents, with complete or near-complete index mean timeseries, are shown in Table 2. (Note that correlations calculated using anomalies are typically much lower than correlations based on 'actual' values, i.e., before a climatology is subtracted, as the latter may be dominated by seasonal variations in temperature. The equivalent results for Table 2 using actual index values are typically >0.9).

Table 2. Mean correlation of value-based indices monthly anomalies for a subset of AR6 regions. Dashes indicate insufficient data to compute correlation.

IPCC AR6 Region	Mean Correlation					
	TXx	TXm	TXn	TNx	TNm	TNn
North-East North America	0.59	0.72	0.49	0.61	0.64	0.43
Southern South America	-	-	-	0.34	0.32	0.14
Northern Europe	0.64	0.76	0.59	0.62	0.69	0.55
West and Central Europe	0.73	0.87	0.70	0.60	0.74	0.69
Russian Arctic	0.65	0.77	0.54	0.64	0.69	0.44
Eastern Asia	0.73	0.73	0.56	0.51	0.69	0.44
Eastern Antarctica	0.29	0.37	0.19	0.27	0.29	0.14

For indices which use daily maximum temperatures (TXx, TXm and TXn), data availability allows correlations to be produced from the monthly anomalies for 19 out of the 46 AR6 land regions, and these range between 0.29 and 0.88 (Figures S2, S8 and S11).

TXx (monthly maximum of daily maximum temperatures) computed for LST tracks air temperature TXx very closely, though LST TXx extremes are predominantly lower than air temperature during winter months (Northern Hemisphere DJF, Southern Hemisphere JJA). During the summer months, the TXx agreement between LST and air temperature is variable, with some regions, such as Northern Europe (NEU) and Western and Central Europe (WCE) (Figures S3b and S4b respectively) regularly displaying air temperature TXx as warmer, whilst for regions such as Eastern Siberia (ESB) (Figure S5b) and the Russian Arctic (RAR) (Figure S6b) LST and air temperature TXx appear more equal or LST is slightly greater. TXn (monthly minimum of daily maximum temperatures) also shows temperatures

are often close, but LST tends to be colder during mid-summer and -winter. A notable exception occurs in the Russian Arctic (RAR) (Figure S9b) region where air temperature TXn is almost always a few degrees cooler than LST TXn at the winter minima. For TXm (monthly mean of daily maximum temperatures), the LST winter minima are typically colder, often by several degrees Celsius, but the LST and air temperature summer maxima are generally quite similar. In East Antarctica (EAN), LST TXx, TXn, and TXm (Figures S7a,b, S10a,b and S12a,b respectively) are almost always colder than air temperature. A similar result is discussed for the Arctic in [30] and is mostly attributed to a negative net radiation balance where the surface cools due to little incoming solar radiation, particularly during the winter and at night. Advection of warm air over the cool surface is also a mechanism that could lead to LST being colder than air temperature [31].

Moving to daily minimum temperature indices (TNx, TNn and TNm), data availability allowed correlations to be calculated for 21/46 AR6 regions, with South-west South America and Southern South America now having sufficient data. The appearance of the South American regions is due to fewer occurrences of deep convection during the night than the day, resulting in more valid LSTs during the 6 am overpass. This is a result of thermal heating and orographic ascent (via the Andes) tending to cause convective storms to form during late afternoon [32,33]. Monthly anomaly correlations for this set of indices range between 0.02 and 0.83 (Figures S13–S15).

For almost all regions, TNx is colder for LST than air temperature during the winter, warmer for LST during the summer, and similar during the spring and autumn months, reflecting a larger annual range of LST. The warmer TNx values during the summer are likely to be due to the more rapid response of LST to insolation (and earlier sunrise timing), whereas air temperature has a much slower response to changes in insolation [34]. Seasonal variation may also be a result of varying surface conditions throughout the year, affecting the penetration depth of the MWs used in LST retrievals. TNn also tracks very well between LST and air temperature with little deviation across most regions over most months. In some regions, air temperature does show a colder winter minimum. The results for TNm are very similar to those of TNn, with some regions also showing air temperature having colder winter minima.

In some regions, there is a clear transition in the value-based indices due to the sensor change from SSM/I to SSMIS in 2009 (Figure 2a), but this may not be present across all indices. For example, in AR6 region North-Eastern North America (NEN), the step change is clear in TXx but not TNn (Figure 3). Good et al. [25] also noted this step change and that this induced a statistically significant non-climatic trend in the combined SSM/I to SSMIS time series. However, it is worth noting that this trend is smaller than the 'minimum requirement to be met to ensure that [LST] data are useful' as defined by the Global Climate Observing System (GCOS) 'threshold' requirement [35]. A similar step change and resulting statistically significant non-climatic trend was also observed in IR LST datasets derived from multiple sensors [25].

3.2. Threshold-Based Indices

All threshold-based indices show a positive correlation between LST and air temperature for all standard threshold-based indices across the 12 AR6 regions (11 regions for TXge35) that have sufficient data to calculate correlations (Figures S16, S17, S25, S28, S30, S32–S34 and S39; a subset of regions are shown in Table 3). Fewer region correlations can be produced for this category of indices because threshold-based indices have an annual frequency, and therefore do not benefit from any monthly-to-seasonal fluctuation in data availability arising from variation in atmospheric dynamics and land surface changes. For relative threshold-based indices, correlations are computable for 20–36 AR6 regions, de-

pending on the index, as a result of applying the lower data availability threshold of 60% (see Section 2.3). Only 11 index-region combinations have negative correlations, although most are not statistically significant.

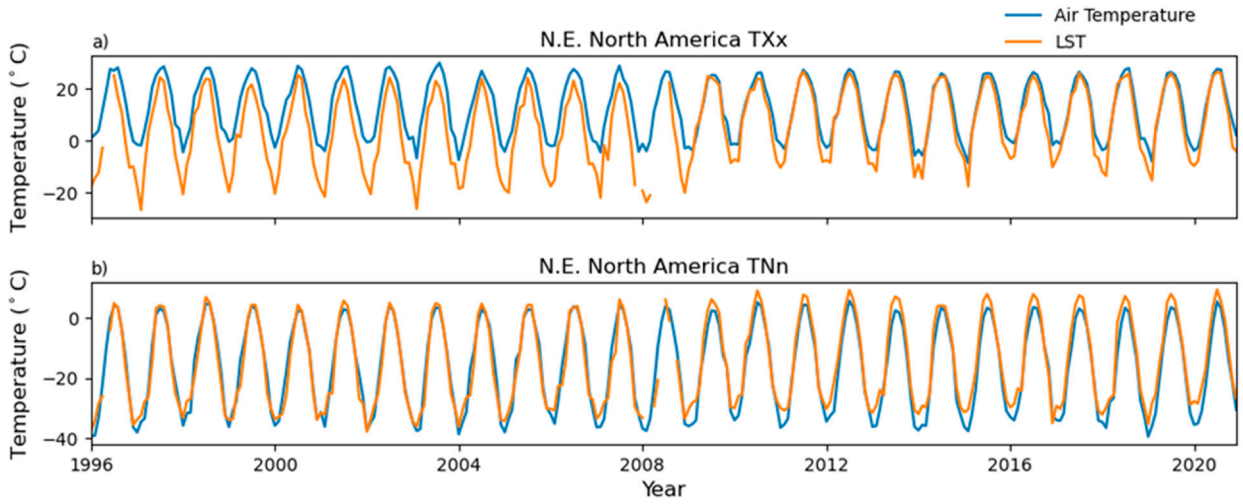


Figure 3. Timeseries of the arithmetic mean results across AR6 region N.E. North America (NEN) for (**a**) TXx and (**b**) TNn.

Table 3. Mean correlation of threshold-based indices for a subset of AR6 regions. Dashes indicate correlations could not be computed. 'Std.' corresponds to the results for indices calculated using the standard approach, whereas 'Rel.' is for the equivalent relative indices (see Section 2.3).

IPCC AR6 Region	Mean Correlation																	
	SU		ID		TR		FD		TNlt2		TNltm2		TNltm20		TXge30		TXge35	
	Std.	Rel.	Std.	Rel.	Std.	Rel.	Std.	Rel.	Std.	Rel.	Std.	Rel.	Std.	Rel.	Std.	Rel.	Std.	Rel.
North-East North America	0.59	0.67	0.95	0.86	0.10	0.03	0.81	0.74	0.79	0.72	0.84	0.77	0.91	0.88	0.45	0.62	0.40	0.34
Central North America	0.73	0.90	0.46	0.88	0.25	0.83	0.60	0.91	0.53	0.92	0.62	0.90	0.57	0.76	0.76	0.89	0.43	0.83
West and Central Europe	0.71	0.72	0.75	0.61	0.52	0.52	0.72	0.65	0.69	0.62	0.79	0.71	0.85	0.75	0.74	0.71	0.56	0.49
Eastern Europe	0.95	0.94	0.82	0.75	0.74	0.74	0.87	0.81	0.87	0.81	0.85	0.83	0.79	0.73	0.95	0.94	0.91	0.90
Russian Arctic	0.79	0.78	0.87	0.80	0.26	0.23	0.78	0.78	0.71	0.72	0.84	0.82	0.92	0.91	0.71	0.70	0.40	0.38
Eastern Asia	-	0.60	-	0.79	-	0.89	-	0.96	-	0.96	-	0.96	-	0.87	-	0.37	-	0.10
Eastern Antarctica	-	-	-	0.71	-	-	-	0.43	-	-	-	0.68	-	0.79	-	-	-	-

The threshold-based indices showing the greatest between-region spread of correlations are, for standard indices, TXge35 (annual number of days when daily maximum temperature is over 35 °C; min = 0.05, max = 0.91) and, for relative indices, TNlt2 (the annual number of days when the daily minimum temperature is under 2 °C; min = −0.16, max = 0.97). Low correlations for both indices in some regions are typically a result of either few events occurring, or a clustering of events at small index values. In addition, Tropical Nights (TR; the annual number of days when the daily minimum temperature exceeds 20 °C) for LST is often observed on many more occasions than air temperature, for example in the Western and Central Europe (WCE) AR6 region (Figure 4). This may be related to the 6am/pm observation time of the MW LST data, which might not occur at the same time as the 'true' minimum LST, particularly for seasons and regions where sunrise occurs before 6am. Therefore, this could result in a more frequent exceedance of the 20 °C threshold in the MW LST data than in the air temperature data.

The Summer Days index (SU), which is the annual number of days that exceed 25 °C, represents a warm moderate extreme. AR6 regions such as West and Central Europe (WCE), Eastern Europe (EEU), the Russian Arctic (RAR) and Eastern Siberia (ESB) show strong similarities in the SU timeseries (Figures S18–S21 (*b* panels) respectively), with standard and relative index correlations between 0.57 and 0.95 and 0.08–0.94 (Figure S17),

respectively. There is usually an offset between the LST and air temperature index values, but their interannual variability is similar.

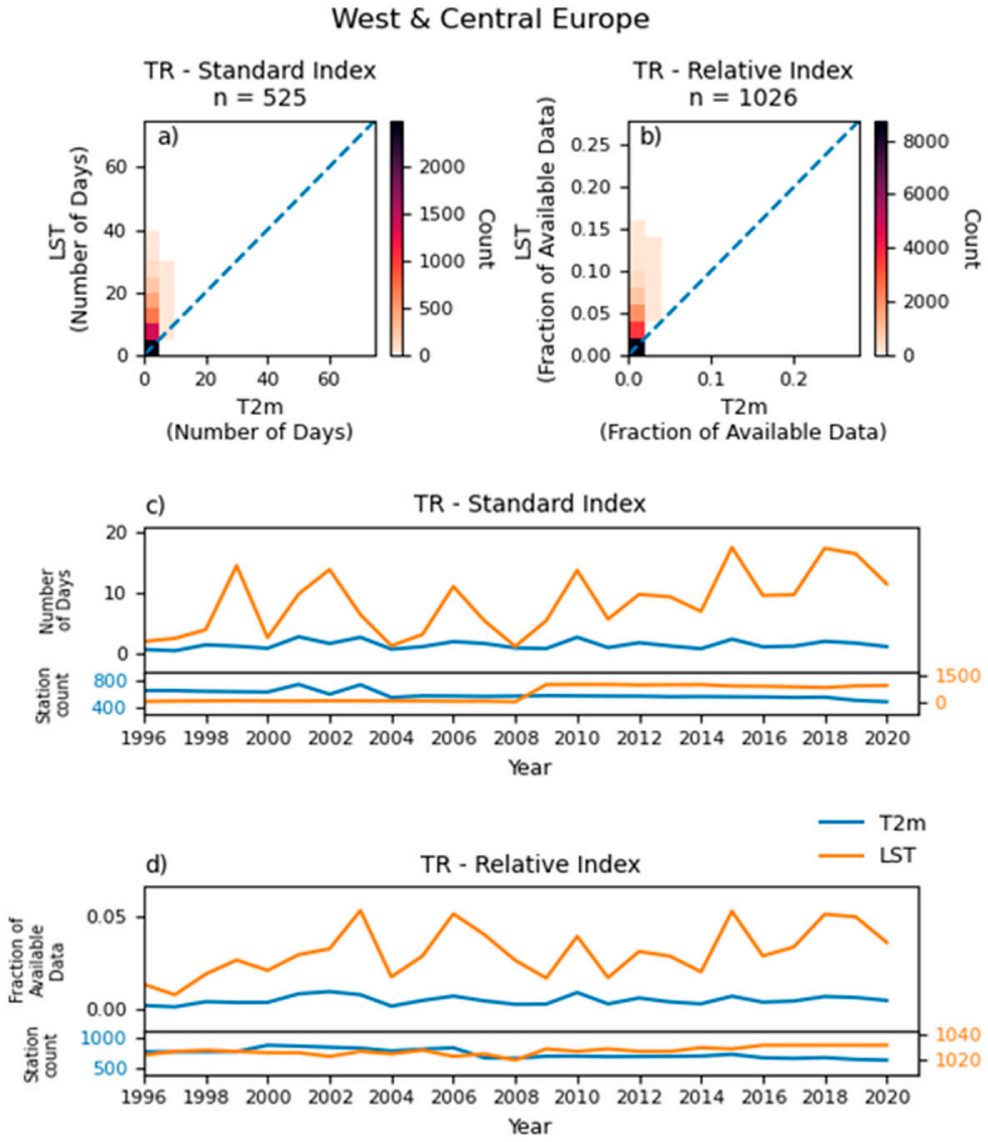


Figure 4. Tropical Nights (TR) standard and relative index density plots (**a**,**b**) and timeseries (**c**,**d**) for the Western-Central Europe (WCE) region. For (**a**,**b**), *n* is the number of contributing stations, and (**c**,**d**) are the standard and relative index arithmetic means, with the number of contributing stations shown in the bottom panels (note the twin *y*-axis). Blue dashed line in (**a**,**b**) is the 1:1 line.

The AR6 regions forming the contiguous United States of America (Western, Central, and Eastern North America—WNA, CNA and ENA) evidence the benefit of using relative indices over the standard construction. Using the standard index, SU values for LST are considerably lower, and the timeseries are only partially complete. However, by converting these to relative indices, a strong temporal tracking between the variables and a reasonably consistent offset is seen (Figures 5 and S22b–S24b). Again, the offset may be a result of the 6 am/pm overpass times not capturing the true LST maximum, causing fewer exceedances of 25 °C.

The correlations between LST and air temperature for Icing Days (ID; daily maximum < 0 °C), Frost Days (FD; daily minimum < 0 °C), TNlt2 (daily minimum < 2 °C) and TNltm2 (daily minimum < -2 °C) are similar (Figures S25, S28, S30 and S32, respectively). Across the four indices, the minimum and maximum standard index correlations are 0.49

(ID in Central North America, Figure S26a) and 0.93 (ID in North-Eastern North America, Figure S27a), respectively, and the minimum and maximum relative index values are −0.16 (TNlt2 in North-Western South America, Figure S31b) and 0.97 (FD in Tibetan Plateau, Figure S29b), respectively. Whilst occurring less frequently in many regions, TNltm20 (daily minimum < −20 °C) events still show high correlations in high-latitude regions (Figure S33), such as across the Eastern Siberia (ESB) region, lying close to the 1:1 line for both the standard and relative index density plots (Figure 6).

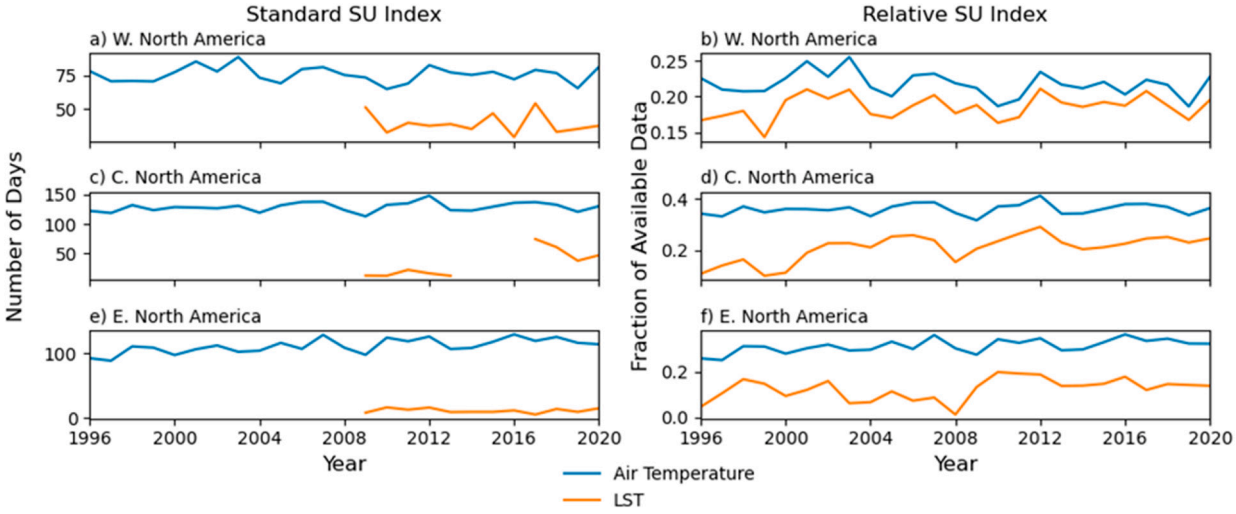


Figure 5. Standard (**a**,**c**,**e**) and relative (**b**,**d**,**f**) SU index for Western (**a**,**b**), Central (**c**,**d**) and Eastern (**e**,**f**) North America.

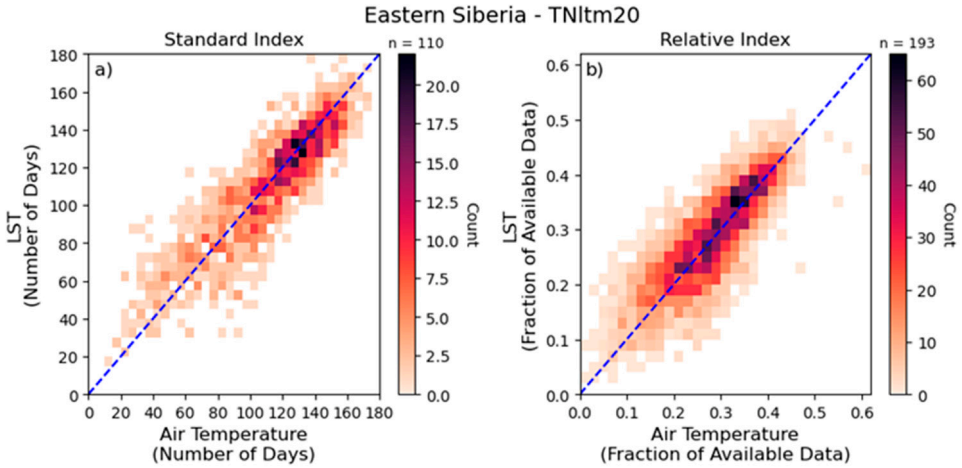


Figure 6. Density plots of TNltm20 for Eastern Siberia (ESB)—(**a**) standard index; (**b**) relative index. *n* is the number of contributing stations, where the relative index uses more stations due to a lower data availability threshold. Blue dashed line in (**a**,**b**) is the 1:1 line.

TXge30 (daily maximum ≥ 30 °C) and TXge35 (daily maximum ≥ 35°) also show high correlations between LST and air temperature indices for some regions, but there is reasonably large variability when looking across all the available regions, particularly for TXge35 (Figures S34 and S39). This is likely due to a combination of these events happening less frequently and occurring in regions prone to more data gaps in LST, such as the tropics. The more highly populated regions where TXge30 and TXge35 relative indices perform well are Western North America (Figures S35a,b and S40a,b), Central North America (Figures S36a,b and S41a,b), West Central Asia (Figures S37a,b and S42a,b) and Eastern Europe (Figures S38a,b and S43a,b).

3.3. Percentile-Based Indices

Percentile-based indices are computed for 19 (21) AR6 regions using the LST daytime (nighttime) overpasses and air temperature maxima (minima). The additional two regions available when using LST nighttime overpasses and air temperature minima are Southwest South America (SWS) and Southern South America (SSA), as before, due to the decrease in convective storms over the Andes during the night (see Section 3.1). The percentile-based indices generally exhibit moderate to high positive correlations between LST and air temperature across all AR6 regions where correlations can be computed (Figures S44–S53, subset shown in Tables 4 and 5).

Table 4. Mean correlation of maximum temperature (TX) percentile-based indices for a subset of AR6 regions.

IPCC AR6 Region	Mean Correlation				
	TX95p	TX90p	TXgt50p	TX10p	TX5p
North-East North America	0.59	0.64	0.65	0.44	0.33
Central North America	0.63	0.67	0.73	0.44	0.38
West and Central Europe	0.74	0.78	0.83	0.77	0.71
Eastern Europe	0.73	0.76	0.81	0.69	0.63
Russian Arctic	0.65	0.71	0.76	0.57	0.48
Eastern Asia	0.54	0.63	0.71	0.57	0.54
Eastern Antarctica	0.10	0.18	0.37	0.17	0.06

Table 5. Mean correlation of minimum temperature (TN) percentile-based indices for a subset of AR6 regions.

IPCC AR6 Region	Mean Correlation				
	TN95p	TN90p	TNlt50p	TN10p	TN5p
North-East North America	0.54	0.64	0.57	0.36	0.27
Central North America	0.54	0.67	0.60	0.37	0.32
West and Central Europe	0.60	0.78	0.64	0.67	0.64
Eastern Europe	0.68	0.76	0.75	0.59	0.52
Russian Arctic	0.59	0.71	0.69	0.46	0.36
Eastern Asia	0.41	0.63	0.62	0.52	0.53
Eastern Antarctica	0.27	0.18	0.28	0.15	0.01

TX95p and TX90p show good consistency in correlations across available AR6 regions, except for Eastern Antarctica, with mean correlations of 0.61 and 0.67 respectively (Figures S44 and S45). The evolution of the TX95p and TX90p timeseries also displays excellent similarity between air temperature and LST. For example, variability in TX90p in the North-Eastern Europe (NEU) and Russian Arctic (RAR) regions is captured by both the air temperature and LST indices with a high degree of coherence (Figure 7a,c). The benefit of percentile-based indices is that they are normalised for each variable and AR6 region, allowing for regional extremes to be more easily identified. Large peaks in the regional timeseries, representing months where a high fraction of days exceed a given percentile, often coincide in the air temperature and LST indices. However, months where either the LST index has a high fraction of days and the air temperature index does not, or vice versa, do occur throughout the timeseries. TX90p and TX95p represent moderate-to-high temperature extremes, and moderate cold extremes are represented by TN10p and TN5p. The mean TN10p correlation between LST and air temperature is 0.48, and 0.42 for TN5p, worse than in TX90 and TX95p. However, the variability seen in air temperature for TN5p and TN10p is also generally well captured in LST (e.g., TX10p in N. Europe and Russian Arctic regions, Figure 7b,d).

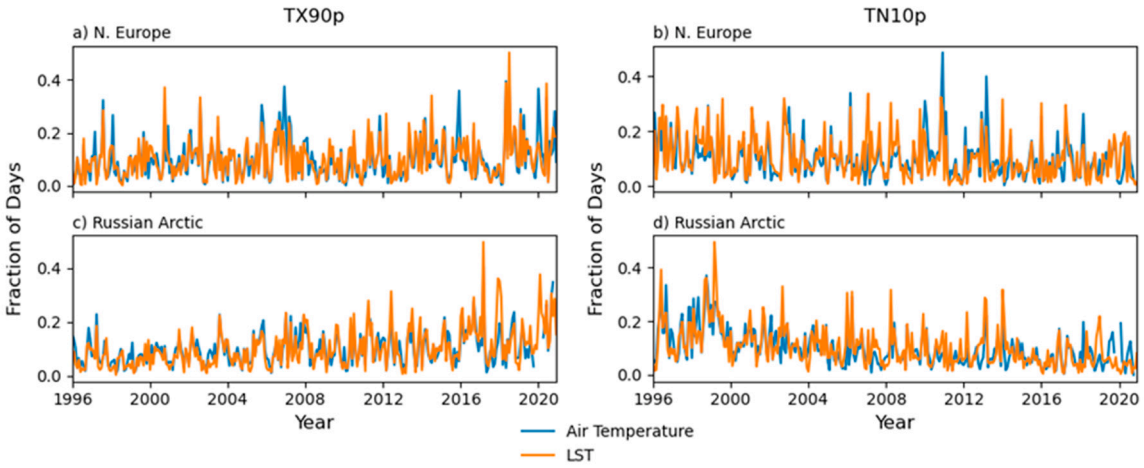


Figure 7. TX90p (**a**,**c**) and TN10p (**b**,**d**) timeseries for the AR6 regions Northern Europe (**a**,**b**) and Russian Arctic (**c**,**d**).

4. Discussion

4.1. Index Comparison

The indices produced for both air temperature and LST show broad agreement for value-, threshold-, and percentile-based indices. There are moderate to strong positive correlations between air temperature and LST across most indices and AR6 regions (see Supplementary Materials). Some neighbouring regions can show differences in the same indices, likely because of each AR6 region having own climate variability and seasonal effects.

Value-based indices have the most consistent high correlations (Figures S2, S8, S11 and S13–S15, Table 2), and this is reflected in the high degree of similarity between the air temperature and LST index values over time, with density plots also regularly showing a near-linear relationship (Figures S3–S7, S9, S10 and S12), and for some index-region combinations lying very close to the 1:1 line (Figure S3). An examination of the regional timeseries reveals that the LST and air temperature value-based indices differ by little during most of the year, with the greatest differences during the summer maxima and winter minima. In regions nearer the equator, such as the tropics, the impact on the relationship between air temperature and LST indices because of less well-defined summer-winter seasons is not possible to assess due to insufficient LST data availability. For regions with adequate data, value-based indices using maximum temperature (TXx, TXn, TXm) tend to show LST with a cold bias in comparison to the air temperature index (see Section 4.2).

The standard threshold-based indices show good performance, with the index correlations largely falling in the range of 0.6–0.8 (Table 3, Figures S16, S17, S25, S28, S30, S32–S34 and S39). The moderately strong correlations for most threshold-based indices demonstrate that LST indices capture similar events to those derived using air temperature, despite using temperature thresholds which were developed for use with air temperature. The exception to this is Tropical Nights (TR), which shows moderately weak correlations for several AR6 regions (Figure S16). Most AR6 regions see more TR events identified from LST than air temperature, with some regions registering several years where the LST index records 40+ tropical nights whilst the air temperature index records 5 or fewer. Large variability in correlations between air temperature and LST can be seen for TXge30 and TXge35 (Figures S34 and S39).

Percentile-based indices utilising maximum temperatures (Figures S44–S48) tend to show greater correlations than those using minimum temperature (Figures S49–S53). These are good correlations for a monthly index, which has a greater degree of influence from climate variability than annual indices. A key feature of the percentile-based indices is that

they self-normalise to each dataset and AR6 region. This can be preferred over value-based indices, as LST and air temperature may respond differently to the levels of insolation and local weather systems [34]; however, they are also more abstract and harder to put into context, especially when averaged over an area. Nevertheless, it is clear that a high degree of variability in the air temperature indices, such as the monthly to annual changes, is also reflected in those calculated from LST. Whilst the index values may be different, a key result is that temperature signals from extreme events are often concurrently visible in both variables (Figure 7). The co-identification of extreme events allows for the possibility of LST to be used as an additional source of climate monitoring alongside the standard air temperature-based indices.

4.2. Reasons for LST and Air Temperature Index Differences

Differences in the index values are expected for a couple of reasons, with three likely causes detailed here.

Firstly, they could be partly due to the potential difference in time of day when acquiring the minimum/maximum temperatures. For air temperature, the true daily minimum/maximum air temperature is used, whereas the LST observations are generally retrieved at 6am or 6pm (see Section 2.2). For example, the maximum LST is more likely to occur between 1 and 3pm, meaning there are a few hours of cooling before the satellite retrieval [34]. This is quite evident in the value-based indices using maximum temperatures (TXx, TXn, TXm), where the LST index value often displayed a cold bias. Additionally, as discussed in Section 3.2, the minimum LST may not be retrieved if sunrise occurs before 6am, depending on the season and region. However, as mentioned previously, temperature extremes may still be identified as they are likely to persist throughout the day, making them noticeable in the timeseries regardless of the measurement time.

Secondly, the index differences between air temperature and LST could also partly be because of the variables being physically different. Whilst the two are related, both conceptually as measures of thermal magnitude, and physically due to land-atmosphere interactions, the thermal properties of a surface can differ significantly from the near-surface air.

Thirdly, a key source of variability is a result of the land-cover type over which LST is retrieved, and how this changes over time. Different land-cover types will heat to varying degrees, and as LST is retrieved over the sensor footprint on the ground (25–35 km), the integrated measurement can be over many different surface types. Where a station is located within this scene will affect the LST and air temperature relationship, and if a scene changes over time (e.g., seasonally), this will further impact how the variables, and the resultant indices, relate to each other.

4.3. Relative Indices

Relative indices (described in Section 2.3) are presented in this study for threshold-based indices (SU, TR, etc.) alongside the standard index values. Standard threshold-based indices are annual counts of days where the daily minimum or maximum temperatures pass given fixed thresholds. For reliable results, these indices require data availability to be high, else missing data may produce an artificially low count.

The data availability limit applied to relative indices in this study is that greater than 60% of a year (219 days) of data must be present. The limit for standard threshold indices used here is approximately 90%, guided in part by the Climpact requirements (see Section 2.3). On average, this constrains standard indices to being reliably produced from LST only between 45 and 60°N; however, relative indices can be calculated between 30 and 70°N and for some areas within 30–45°S as well (Figure 2c). In AR6 regions with sufficient data to produce informative density plots, i.e., often Northern Europe, West and Central

Europe, and the regions covering Russia, the distribution of index values produced by the standard and relative indices show excellent correlation (e.g., TNltm20 for Eastern Siberia (ESB, Figure 6), and SU for Central North America (CNA, Figure S23). This demonstrates that despite relative indices requiring less data, the information captured by them still broadly reflects that captured by the standard indices.

Relative indices also appear to provide greater consistency in the differences between the air temperature and LST index values, particularly when considering the microwave sensor change from SSM/I to SSMIS in 2009, as can be seen in the SU index timeseries for the Eastern Europe (EEU) and Western North America (WNA) AR6 regions (Figures S19 and S22, respectively). Relative indices can also better display notable events than the standard indices within the LST timeseries. For example, the European heatwaves in 2003 [36] and the 2010 Russian heatwave [37] are visible in SU using the relative index for Western-Central Europe (WCE) and Eastern Europe (EEU), respectively (Figure 8).

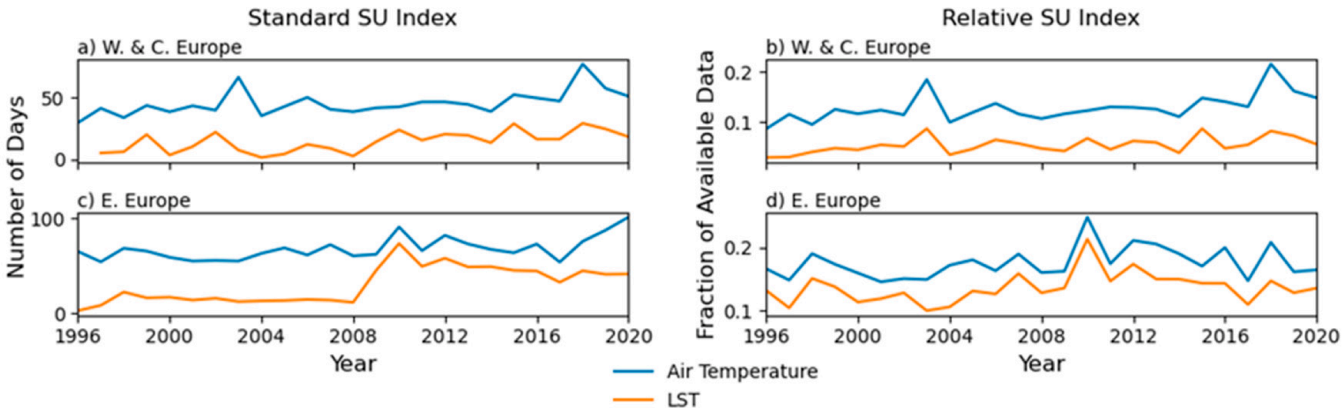


Figure 8. Timeseries of the arithmetic mean for West and Central Europe (WCE), (**a**) standard SU, (**b**) relative SU, and Eastern Europe (EEU), (**c**) standard SU, and (**d**) relative SU.

Currently, producing standard indices for regions across the tropics can be difficult due to fewer stations and less polar-orbiting satellite coverage. However, as relative indices capture much of the information provided by standard indices and significant events can still be identified, these have the potential to provide complementary information across less well-observed areas. Further work should be undertaken to determine a lower threshold on the data availability required to retain a suitable amount of information and how regions with seasonal coverage may be affected. This work enforces 60% data availability, but if similar results can be obtained with less data, gridded indices for station-sparse areas such as North and Central Africa could be produced using LST from polar-orbiting satellites. This would provide a greater capability for monitoring the climate and identifying temperature extremes in these regions, which are vulnerable to the impacts of climate change [38,39].

4.4. Dataset Development and Uncertainties

A follow-on to this study would be the development of an LST-based temperature indices product for use by interested communities and stakeholders, such as researchers, policy makers, and industry. Consultations with potential users would guide the direction and content of the product. A common request for climate datasets is the inclusion of uncertainty estimates, and this section briefly describes how these may be incorporated into an LST indices product, though this is purely conceptual and uncertainties are not provided in this manuscript and remain as future work.

The LST_cci MW product is supplied with estimates of uncertainties on the observations. For value-based indices, their uncertainty ranges would be found by calculating the

index after separately adding and subtracting the uncertainty from the observed value. Using TXx (monthly maximum of the daily maximum temperatures) as an example, the upper bound would be the monthly maximum temperature produced from the sum of the daily observations and their respective uncertainties, whilst the lower bound would be the monthly maximum of the daily observations minus their respective uncertainties.

Similarly, an uncertainty range on the threshold-based indices could be found by considering the index threshold as a fixed value with no uncertainty, and again using the observation uncertainties to produce a range of potential values and computing upper- and lower-bounds on the indices.

Lastly, uncertainties on the percentile-based indices would follow a similar process to that of the threshold-based indices, using the percentile as a fixed value and finding the monthly fraction of days that surpass it after adding and subtracting observational uncertainties from the observations. However, there would also be an associated uncertainty on the computed percentile values, which adds complexity and would need to be calculated and propagated to produce a full uncertainty budget.

5. Limitations and Future Development

This study presents an initial investigation into producing climate indices using LST data. Whilst the results show that there is potential and value in producing LST-based indices, there are items to be addressed before development and deployment of an operational dataset.

Firstly, the satellite overpass times of 6am/pm used to derive LST present a limitation that would impact the performance of threshold-based indices. If the LST maximum and minimum temperatures do not occur near these times, the LST indices produced may not be a true reflection of whether an index was triggered at some other period of the day, making the comparison with NSAT indices less reliable. Future work could make use of LST from geostationary satellites, which have a greater temporal frequency, meaning daily LST minima and maxima will be closer to the truth, and/or the development of LST-specific indices more suitable to the current overpass times.

Secondly, as noted previously, satellite sensor changes can induce non-climatic discontinuities and trends. Whilst the trend from the microwave LST used in this study is within the GCOS 'threshold' requirement, resulting trends in LST indices should be carefully assessed and interpreted. Minimising these trends should be strongly considered when developing an LST indices dataset, as well as working with satellite LST data developers to reduce the discontinuity at the source.

Thirdly, this study presents some initial ideas of how to make LST indices most beneficial, particularly through using relative indices, but future work to determine the optimum data availability should be carried out prior to dataset development. A coverage threshold of 60% is used in this work, but a sensitivity analysis on the proportion of missing data allowed could be carried out to maximise the global coverage whilst ensuring the LST indices are robust. Future work could also include a sensitivity analysis on the missing data thresholds used for the standard indices, which are guided by the Climpact requirements.

Finally, any dataset based on LST indices needs to be evaluated to ensure extreme events are captured accurately, for example, by using an event-based validation. In this case, validation needs to be carried out carefully, and on a grid-cell-by-grid-cell basis rather than using the AR6 regions adopted here, which may not correspond to the geographical area(s) affected by a given extreme event.

6. Conclusions

The results presented in this study evaluate the concept of using LST-based indices for climate monitoring. A selection of standard climate indices is presented from ETCCDI and ET-SCI, together with relative indices to account for data gaps. The results show that there is often a high degree of correlation between indices calculated from air temperature and those from LST. The correlations between air temperature and LST indices vary between AR6 regions for a variety of reasons, but a clear limitation is comparing air temperature maximum (minimum) with LST 6pm (6am) observations. However, the approach presented is motivated by the hypothesis that an extreme temperature event would persist throughout a day, such that for certain indices the signal of this event would be present despite different measurement times. This can be seen when using the relative indices, and it is demonstrated how two historical heatwaves could be identified from both air temperature and LST. Nevertheless, challenges resulting from the overpass times and any sensor changes reduce the reliability of the LST indices. Further work to evaluate and resolve these issues should be carried out before an operational dataset is produced. Options include investigating LST from geostationary satellites and LST-specific indices, as discussed in Section 5.

Value-based index anomalies show good correlation between air temperature and LST, and percentile-based indices show strong similarities in the monthly to annual variability. Threshold-based indices from LST often closely track those produced using air temperature, with differences mainly occurring at maximum and minimum temperatures.

As these results show good potential for the use of LST-based climate indices, a future dataset is proposed to provide these indices and their associated uncertainties.

Supplementary Materials: The following supporting information can be downloaded at: https://www.mdpi.com/article/10.3390/rs18213815/s1, Figures S1–S53. Figures prepended with an "S" can be found in the Supplementary Materials.

Author Contributions: Conceptualization, E.G.; methodology, E.G. and J.B.; software, J.B.; formal analysis, J.B. and E.G.; data curation, C.J.; writing—original draft preparation, J.B.; writing—review and editing, E.G., C.J. and A.C.; visualisation, J.B.; supervision, E.G.; project administration, E.G.; funding acquisition, E.G. All authors have read and agreed to the published version of the manuscript.

Funding: This study has been funded through the European Space Agency (ESA) within the framework of the Land Surface Temperature project under the Climate Change Initiative (LST_cci), contract number 4000123553/18/I-NB, and the U.K.–China Research and Innovation Partnership Fund through the Met Office Climate Science for Service Partnership (CSSP) China under the International Science Partnerships Fund (ISPF).

Data Availability Statement: Near-surface air temperature data were retrieved from the Global Historical Network daily [19] using the Global Summary of the Day: https://www.ncei.noaa.gov/products/land-based-station/global-historical-climatology-network-daily (accessed on 31 August 2023). Daily satellite (ascending and descending) microwave land surface temperature data were acquired from the European Space Agency Land Surface Temperature Climate Change Initiative (ESA LST_cci) [22]: https://catalogue.ceda.ac.uk/uuid/a7e811fe11d34df5abac6f18c920bbeb/ (accessed on 10 August 2024). IPCC AR6 region data [22] were downloaded from: https://zenodo.org/records/5171760 (accessed on 15 August 2024). Using these data with the software provided in [27], reproduces the results presented in this study.

Acknowledgments: The authors are grateful to the ESA for creating the CCI program, which has strengthened the consistency of the many research communities related to developing, processing, qualifying, and using satellite climate data records. We would also like to extend our thanks to Anke Tetzlaff for helpful discussions and insights regarding the use of LST for climate indices. Finally, thank you to the three anonymous reviewers for providing insightful and constructive feedback.

Conflicts of Interest: Author Carlos Jimenez was employed by the company Estellus. The remaining authors declare that the research was conducted in the absence of any commercial or financial relationships that could be construed as a potential conflict of interest.

Abbreviations

The following abbreviations are used in this manuscript:

NSAT	Near-Surface Air Temperature
LST	Land Surface Temperature

References

1. Intergovernmental Panel on Climate Change (IPCC). Weather and Climate Extreme Events in a Changing Climate. In *Climate Change 2021—The Physical Science Basis: Working Group I Contribution to the Sixth Assessment Report of the Intergovernmental Panel on Climate Change*; Cambridge University Press: Cambridge, UK, 2023; pp. 1513–1766. [CrossRef]
2. Dunn, R.J.H.; Blannin, J.; Willett, K.M.; Gobron, N.; Morris, G.A.; Ades, M.; Adler, R.; Alexe, M.; Allan, R.P.; Anderson, J.; et al. Global Climate [in "State of the Climate in 2024"]. *Bull. Amer. Meteor. Soc.* **2025**, *106*, S11–S172. [CrossRef]
3. Dunn, R.J.H.; Alexander, L.V.; Donat, M.G.; Zhang, X.; Bador, M.; Herold, N.; Lippmann, T.; Allan, R.; Aguilar, E.; Barry, A.A.; et al. Development of an updated global land in situ-based data set of temperature and precipitation extremes: HadEX3. *J. Geophys. Res. Atmos.* **2020**, *125*, e2019JD032263. [CrossRef]
4. Huynen, M.; Martens, M.; Schram, P.; Weijenberg, D.; Kunst, M.P. The impact of heat waves and cold spells on mortality rates in the Dutch population. *Environ. Health Perspect.* **2001**, *109*, 463–470. [CrossRef] [PubMed]
5. García-Herrera, R.; Díaz, J.; Trigo, R.M.; Luterbacher, J.; Fischer, E.M. A Review of the European Summer Heat Wave of 2003. *Crit. Rev. Environ. Sci. Technol.* **2010**, *40*, 267–306. [CrossRef]
6. Bishop-Williams, K.E.; Berke, O.; Pearl, D.L.; Hand, K.; Kelton, D.F. Heat stress related dairy cow mortality during heat waves and control periods in rural Southern Ontario from 2010–2012. *BMC Vet. Res.* **2015**, *11*, 291. [CrossRef] [PubMed]
7. Barnabás, B.; Jäger, K.; Fehér, A. The effect of drought and heat stress on reproductive processes in cereals. *Plant Cell Environ.* **2008**, *31*, 11–38. [CrossRef] [PubMed]
8. Reyer, C.P.O.; Leuzinger, S.; Rammig, A.; Wolf, A.; Bartholomeus, R.P.; Bonfante, A.; de Lorenzi, F.; Dury, M.; Gloning, P.; Jaoudé, R.A.; et al. A plant's perspective of extremes: Terrestrial plant responses to changing climatic variability. *Glob. Change Biol.* **2013**, *19*, 75–89. [CrossRef] [PubMed]
9. Forzieri, G.; Bianchi, A.; Batista E Silva, F.; Herrera, M.A.M.; Leblois, A.; Lavalle, C.; Aerts, J.C.J.H.; Feyen, L. Escalating impacts of climate extremes on critical infrastructures in Europe. *Glob. Environ. Change* **2018**, *48*, 97–107. [CrossRef] [PubMed]
10. Zhang, Y.; Seidel, D.J.; Golaz, J.C.; Deser, C.; Tomas, R.A. Climatological characteristics of Arctic and Antarctic surface-based inversions. *J. Clim.* **2011**, *24*, 5167–5186. [CrossRef]
11. Frich, P.; Alexander, L.V.; Della-Marta, P.; Gleason, B.; Haylock, M.; Klein Tank, A.M.G.; Peterson, T. Observed coherent changes in climatic extremes during the second half of the twentieth century. *Clim. Res.* **2002**, *19*, 193–212. [CrossRef]
12. Donat, M.G.; Alexander, L.V.; Yang, H.; Durre, I.; Vose, R.; Caesar, J. Global Land-Based Datasets for Monitoring Climatic Extremes. *Bull. Am. Meteorol. Soc.* **2013**, *94*, 997–1006. [CrossRef]
13. Dunn, R.J.H.; Herold, N.; Alexander, L.V.; Donat, M.G.; Allan, R.; Bador, M.; Brunet, M.; Cheng, V.; Ibadullah, W.M.W.; Bin Ibrahim, M.K.I.; et al. Observed global changes in sector-relevant climate extremes indices—An extension to HadEX3. *Earth Space Sci.* **2024**, *11.4*, e2023EA003279. [CrossRef]
14. Ghent, D.J.; Corlett, G.K.; Göttsche, F.M.; Remedios, J.J. Global land surface temperature from the along-track scanning radiometers. *J. Geophys. Res. Atmos.* **2017**, *122*, 12–167. [CrossRef]
15. Menne, M.J.; Durre, I.; Vose, R.S.; Gleason, B.E.; Houston, T.G. An overview of the global historical climatology network-daily database. *J. Atmos. Ocean. Technol.* **2012**, *29*, 897–910. [CrossRef]
16. Iturbide, M.; Gutiérrez, J.M.; Alves, L.M.; Bedia, J.; Cerezo-Mota, R.; Cimadevilla, E.; Cofiño, A.S.; Di Luca, A.; Faria, S.H.; Gorodetskaya, I.V.; et al. An update of IPCC climate reference regions for subcontinental analysis of climate model data: Definition and aggregated datasets. *Earth Syst. Sci. Data* **2020**, *12*, 2959–2970. [CrossRef]
17. Intergovernmental Panel on Climate Change (IPCC). *Climate Change 2021—The Physical Science Basis: Working Group I Contribution to the Sixth Assessment Report of the Intergovernmental Panel on Climate Change*; Cambridge University Press: Cambridge, UK, 2023. [CrossRef]
18. Iturbide, M.; Fernández, J.; Gutiérrez, J.M.; Bedia, J.; Cimadevilla, E.; Díez-Sierra, J.; Manzanas, R.; Casanueva, A.; Baño-Medina, J.; Milovac, J.; et al. *Repository Supporting the Implementation of FAIR Principles in the IPCC-WGI Atlas, v2.0-Final*; Zenodo: Geneva, Switzerland, 2021. [CrossRef]

19. Duan, S.; Han, X.; Huang, C.; Li, Z.; Wu, H.; Qian, Y.; Gao, M.; Leng, P. Land Surface Temperature Retrieval from Passive Microwave Satellite Observations: State-of-the-Art and Future Directions. *Remote Sens*. **2020**, *12*, 2573. [CrossRef]
20. Perry, M.; Ghent, D.J.; Jiménez, C.; Dodd, E.M.A.; Ermida, S.L.; Trigo, I.F.; Veal, K.L. Multisensor Thermal Infrared and Microwave Land Surface Temperature Algorithm Intercomparison. *Remote Sens*. **2020**, *12*, 4164. [CrossRef]
21. Prigent, C.; Aires, F.; Rossow, W.B. Land surface skin temperatures from a combined analysis of microwave and infrared satellite observations for an all-weather evaluation of the differences between air and skin temperatures. *J. Geophys. Res*. **2003**, *108*, 4310. [CrossRef]
22. Jimenez, C.; Prigent, C. *ESA Land Surface Temperature Climate Change Initiative (LST_cci): All-Weather MicroWave Land Surface Temperature (MW-LST) Global Data Record (1996–2020), v2.33*; NERC EDS Centre for Environmental Data Analysis: Swindon, UK, 2023. [CrossRef]
23. Ghent, D.; Dodd, E.; Veal, K.; Perry, M.; Jimenez, C.; Ermida, S. *ESA Land Surface Temperature Climate Change Initiative (LST_cci): Algorithm Theoretical Basis Document (Version 4.2)*; European Space Agency (ESA): Paris, France, 2025.
24. Ghent, D.; Ermida, S.; Jimenez, C.; Dodd, E. *ESA Land Surface Temperature Climate Change Initiative (LST_cci): Product User Guide (Version 3.1)*; European Space Agency (ESA): Paris, France, 2024.
25. Good, E.J.; Aldred, F.M.; Ghent, D.J.; Veal, K.L.; Jimenez, C. An analysis of the stability and trends in the LST_cci Land Surface Temperature datasets over Europe. *Earth Space Sci*. **2022**, *9*, e2022EA002317. [CrossRef]
26. Zhang, X.; Hegerl, G.; Zwiers, F.; Kenyon, J. Avoiding Inhomogeneity in Percentile-Based Indices of Temperature Extremes. *J. Clim*. **2005**, *18*, 1641–2165. [CrossRef]
27. Blannin, J. LST Climate Indices [Software]. Github. 2026. Available online: https://github.com/MetOffice/LST_Climate_Indices (accessed on 14 October 2026).
28. Herold, N.; Alexander, L. Climpact v3.3. 2025. Available online: https://github.com/ARCCSS-extremes/climpact (accessed on 6 May 2025).
29. Cheda, A.; Tetzlaff, A.; Blannin, J.; Good, E.; Sharma, V.; Trigo, I.; Schwaab, J.; Riihelä, A.; Grams, C.M.; Schröder, M. Heat Indices for Europe Derived from Satellite Data: A Proof of Concept. *Remote Sens*. **2026**, *18*, 589. [CrossRef]
30. Nielsen-Englyst, P.; Høyer, J.L.; Madsen, K.S.; Tonboe, R.; Dybkjær, G.; Alerskans, E. In situ observed relationships between snow and ice surface skin temperatures and 2 m air temperatures in the Arctic. *Cryosphere* **2019**, *13*, 1005–1024. [CrossRef]
31. Zhang, X.; Alexander, L.; Hegerl, G.C.; Jones, P.; Klein Tank, A.; Peterson, T.C.; Trewin, B.; Zwiers, F.W. Indices for monitoring changes in extremes based on daily temperature and precipitation data. *WIREs Clim. Change* **2011**, *2*, 851–870. [CrossRef]
32. Riley Dellaripa, E.M.; Maloney, E.D.; DeMott, C.A. The diurnal cycle of east Pacific convection, moisture, and CYGNSS wind speed and fluxes. *J. Geophys. Res. Atmos*. **2023**, *128*, e2022JD038133. [CrossRef]
33. Kirshbaum, D.J.; Adler, B.; Kalthoff, N.; Barthlott, C.; Serafin, S. Moist orographic convection: Physical mechanisms and links to surface-exchange processes. *Atmosphere* **2018**, *9*, 80. [CrossRef]
34. Good, E.J. An in situ-based analysis of the relationship between land surface "skin" and screen-level air temperatures. *J. Geophys. Res. Atmos*. **2016**, *121*, 8801–8819. [CrossRef]
35. World Meteorological Organization (WMO); Intergovernmental Oceanographic Commission of the United Nations Educational, Scientific and Cultural Organization (IOC-UNESCO); International Science Council (ISC); United Nations Environment Programme (UNEP); Copernicus Climate Change Service (C3S). GCOS Report-245 "The 2022 GCOS ECVs Requirements 2022 edition"—Updated in 2025. 2025. Available online: https://library.wmo.int/idurl/4/58111 (accessed on 1 June 2026).
36. Stott, P.A.; Stone, D.A.; Allen, M.R. Human contribution to the European heatwave of 2003. *Nature* **2004**, *432*, 610–614. [CrossRef] [PubMed]
37. Trenberth, K.E.; Fasullo, J.T. Climate extremes and climate change: The Russian heat wave and other climate extremes of 2010. *J. Geophys. Res. Atmos*. **2012**, *117*, D17103. [CrossRef]
38. Schilling, J.; Hertig, E.; Tramblay, Y.; Scheffran, J. Climate change vulnerability, water resources and social implications in North Africa. *Reg. Environ. Change* **2020**, *20*, 15. [CrossRef]
39. Diedhiou, A.; Bichet, A.; Wartenburger, R.; Seneviratne, S.I.; Rowell, D.P.; Sylla, M.B.; Diallo, I.; Todzo, S.; E Touré, N.; Camara, M.; et al. Changes in climate extremes over West and Central Africa at 1.5 C and 2 C global warming. *Environ. Res. Lett*. **2018**, *13*, 065020. [CrossRef]

Disclaimer/Publisher's Note: The statements, opinions and data contained in all publications are solely those of the individual author(s) and contributor(s) and not of MDPI and/or the editor(s). MDPI and/or the editor(s) disclaim responsibility for any injury to people or property resulting from any ideas, methods, instructions or products referred to in the content.